An Inter-Subband Device with Terahertz Applications

Philip D. Buckle, Philip Dawson, Mark A. Lynch, Chun-Yi Kuo, Mohammed Missous, and William S. Truscott

***Abstract*—A theoretical analysis of a modulator based on two coupled resonators is presented in this paper. This modulator exhibits a resonant enhancement in its response. It is used as a component of tunneling structures designed for operation at terahertz frequencies; unlike conventional resonant tunneling structures, these use triple barriers. Data from optical and electrical measurements on a series of devices based on one design of a triple-barrier tunneling structure have been analyzed to estimate their behavior at frequencies over 1 THz. The analysis gives values for the resonantly enhanced admittance, its bandwidth, the bias–frequency relationship, and the requirements for a matching circuit to a 50-Ω environment. The results show that one existing structure might be used in oscillators working at 1 THz.**

***Index Terms*—Inter-subband devices, microwave filters, modulators, resonant tunneling, terahertz oscillators, triple-barrier devices.**

I. Introduction

DETAILED quantum mechanical modeling has shown that triple-barrier tunneling structures can act as electrically excited terahertz sources. Terahertz operation is based on an inter-subband resonance and depends on the applied bias producing the correct subband alignment [1]. This paper presents an analysis of this behavior in the terminology of microwave filters that are mathematically equivalent. The results of optical and electrical measurements on a series of triple-barrier structures are then presented and used to establish the conditions under which a resonant enhancement of the negative conductance should be observed. The data show that many of the necessary criteria for terahertz operation have been met in some of these structures.

II. Theory of a Resonant Modulator

The inter-subband devices that are the subject of this paper are designed to operate at terahertz frequencies by means of a combination of quantum mechanical and physical electronic processes. These processes are used, respectively, to modulate an electron current and to provide power gain in distinct regions of the device. In order to present the case that some existing triple-barrier structures meet or nearly meet the requirements for successful terahertz operation, a discussion of the quantum electronic aspects of the device operation is included. An account of the quantum processes is given in terms close to those of microwave filter engineering; this presentation shows that the novel ideas used in the triple-barrier devices could also be applied in the high-frequency modulation of microwave carriers.

The objective of using triple-barrier structures is to overcome the frequency limitations for the operation of more conventional double-barrier resonant tunneling structures (DBRTS's); the development of these seems to have reached fundamental material and structural limitations that restrict their operation to frequencies below 1 THz [2]. The section of the device that modulates the electron current exploits a quantum resonance within the triple-barrier region of the device to overcome dynamic limitations associated with the electron mass. These limitations restrict the frequency at which the rate of electron tunneling through more conventional devices can be modulated. There is a direct equivalence between the equations for the multibarrier quantum system and those for multipole microwave filters. The quantum system acts as a modulator with a resonant enhancement of its gain; by using equivalent principles and design features, these concepts could be applied to multipole microwave structures enabling them to operate as effective modulators. The authors propose that the quantum effect exploited in the terahertz devices should be named quantum modulation in scattering and tunneling (QMIST)—the QMIST effect.

The triple-barrier structures consist of alternate layers of GaAs and $Al_xGa_{1-x}As$, an alloy with a larger bandgap that acts as a barrier to the flow of electrons between the layers of GaAs. Fig. 1 shows the variation with distance of the minimum energy for electrons in the device under bias. It also shows (in insets) a waveguide filter with many equivalent properties and a graph of the electron transmission probability as a function of energy; this probability is equivalent to s_{21} for the waveguide filter. This filter is composed of a sequence of waveguide sections, with alternating lower and higher cutoff frequencies: if the lengths of the low cutoff frequency sections that act as resonators between the portions of narrower waveguide are correctly chosen, a filter with two pole pairs at specific frequencies will be produced. The coupling of the modes and their bandwidths depends on the dimensions of the narrower portions that will be cutoff over the operating frequency range. If the incoming wave at the frequency of the mode mainly associated with the first resonator is modulated and the modulation frequency increased, the degree of modulation of the transmitted wave will fall when the bandwidth of this first mode is exceeded, but will recover, at least in part, when the modulation frequency is such as to allow the second mode to pass one of the sidebands of the modulation. The relative phase of the modulation of the transmitted wave will depend on the phase shift associated with this second mode and, hence, on the frequency of the modulation in comparison with the splitting of the two modes.

Manuscript received March 1, 1999. This work was supported by the Engineering and Physical Sciences Research Council under Grant GR/J 78 013.

P. D. Buckle, M. A. Lynch, C.-Y. Kuo, M. Missous, and W. S. Truscott are with the Department of Electrical Engineering and Electronics, University of Manchester Institute of Science and Technology, Manchester M60 1QD, U.K.

P. Dawson is with the Department of Physics, University of Manchester Institute of Science and Technology, Manchester M60 1QD, U.K.

Publisher Item Identifier S 0018-9480(00)02520-5.

0018–9480/00$10.00 © 2000 IEEE

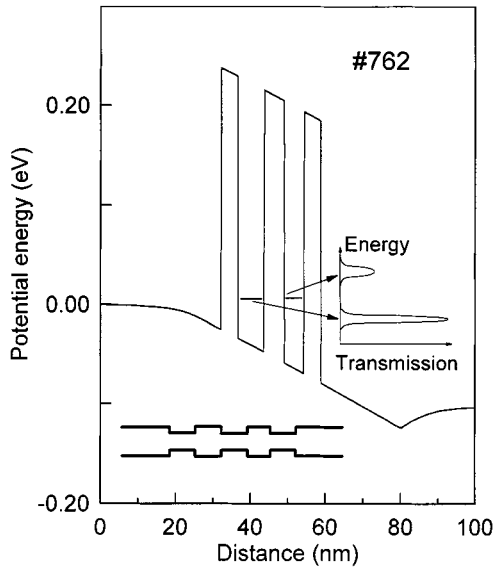

Fig. 1. Calculated plot of the minimum energy for electrons in the conduction band as a function of distance across the active region of a triple-barrier structure similar to #762 showing the three $Al_xGa_{1-x}As$ barriers. The lines in each of the quantum wells show the energies of the lowest resonant states. The diagram is drawn for a forward bias of 0.1 V, which brings the energies of the two states within 6 meV (1.5 THz). The inset to the right-hand side shows, as a function of energy on an expanded scale, a sketch of the probability for electron transmission, indicating the peaks associated with the two resonant states. The inset at the bottom shows a sketch of an equivalent waveguide structure that also has a pair of resonant modes; the waveguide equivalent to transmission probability is s_{21}.

The triple-barrier structure acts as an energy-selective filter for electrons in a very similar fashion to a four-pole waveguide filter, with two pass energies whose splitting is determined by the thicknesses of the layers of different materials and the bias applied to the device. The emitter region of the device acts as a source of electron waves with a wide spread of energies; only those electrons with energies within the two resonances are transmitted. By correctly designing the widths of the barriers, it is possible to arrange that the mode associated with the first quantum well has the longer lifetime, in which case, it will dominate the transmission characteristics since the transmission coefficient integrated over the range of the resonance will be greater than that for the wider resonance.

If the time and space dependence of the mode in the first resonator or quantum well, when it is solely coupled to the incoming section and not to the second, is given by the function $\Psi_1(x) \cdot \exp(j\omega_1 t - \Gamma_1 t)$ and that in the second by $\Psi_2(x) \cdot \exp(j\omega_2 t - \Gamma_2 t)$ under the same conditions, and the two resonators or wells are coupled through the central section by a coupling of strength ω_c, then the coupled modes a and b can be obtained by diagonalizing the matrix equation describing the coupled time evolution to give

$$\Psi_a = \Big[\alpha\Psi_1(x) + \beta\Psi_2(x)\Big]\exp(j\omega_a t - \Gamma_a t)$$

and

$$\Psi_b = \Big[-\beta^*\Psi_1(x) + \alpha^*\Psi_2(x)\Big]\exp(j\omega_b t - \Gamma_b t)$$

with

$$\alpha/\beta = r + (1+r^2)^{\frac{1}{2}}$$

and

$$r = (\omega_1 - \omega_2 + j\Gamma_1 - j\Gamma_2)/\omega_c$$

with

$$\begin{aligned} 2(j\omega_a - \Gamma_a) = {} & j\omega_1 + j\omega_2 - \Gamma_1 - \Gamma_2 + \beta^*\beta \\ & \cdot \Big[(\alpha^*\alpha/\beta^*\beta - 1)(j\omega_1 - j\omega_2 - \Gamma_1 + \Gamma_2) \\ & + (\alpha^*/\beta^* + \alpha/\beta)\omega_c\Big] \end{aligned}$$

and

$$\begin{aligned} 2(j\omega_b - \Gamma_b) = {} & j\omega_1 + j\omega_2 - \Gamma_1 - \Gamma_2 - \beta^*\beta \\ & \cdot \Big[(\alpha^*\alpha/\beta^*\beta - 1)(j\omega_1 - j\omega_2 - \Gamma_1 + \Gamma_2) \\ & + (\alpha^*/\beta^* + \alpha/\beta)\omega_c\Big]. \end{aligned}$$

As a result of the coupling, the two eigenmodes are no longer restricted to one resonator or well, but have a finite amplitude in each section that depends on r, the ratio of the difference in the time dependence of the two modes to the coupling frequency. The above equations describe the time-independent system: if a wave of constant amplitude is incident onto the first barrier or cutoff section, the resultant amplitudes throughout the system can be found, including the amplitude of the wave that has passed through the final barrier or cutoff section. This will be proportional to the amplitude of the wave in the second resonator or quantum well and, in the case of electron tunneling, the tunneling current will be proportional to the square of this amplitude.

In devices that are subject to a sinusoidal time-dependent bias $\cos(\omega_m t)$, whose scale is described by a small parameter λ, the term $(\omega_1 - \omega_2)$ in the above equations will become $[\omega_1 - \omega_2 + \lambda\Omega \cdot \cos(\omega_m t)]$. Since one of the terms in the matrix equation has changed, the transformation $[\alpha, \beta; -\beta^*, \alpha^*]$ to the basis Ψ_a and Ψ_b no longer diagonalizes the matrix equation. In that representation, the additional term adds a diagonal perturbation to $j\omega_a$ (or $j\omega_b$) of $\pm j\lambda(\alpha^*\alpha - \beta^*\beta)\Omega \cdot \cos(\omega_m t)/2$ and off-diagonal terms $-j\lambda\alpha\beta\Omega\cdot\cos(\omega_m t)$, which will mix Ψ_a and Ψ_b. Since this latter term is time dependent, the time-dependent wave equation must be solved explicitly. A trial solution $\Psi_P = [A(t)\Psi_a(x) + B(t)\Psi_b(x)]\exp(j\omega_P t - \Gamma_P t)$ is substituted into the time-dependent wave equation

$$\begin{aligned} & \partial\Psi_P(x,t)/\partial t \\ & \quad = \Big[\partial A(t)/\partial t\Psi_a(x) + (j\omega_P t - \Gamma_P)A(t)\Psi_a(x) \\ & \qquad + \partial B(t)/\partial t\Psi_b(x) + (j\omega_P t - \Gamma_P)B(t)\Psi_b(x)\Big] \\ & \qquad \times \exp(j\omega_P t - \Gamma_P t) \\ & \quad = \Bigg\{\Big[(j\omega_a - \Gamma_a) + j\lambda(\alpha^*\alpha - \beta^*\beta)\Omega\cos(\omega_m t)/2\Big] \\ & \qquad \cdot A(t)\Psi_a(x) - j\lambda\alpha\beta\Omega\cos(\omega_m t)A(t)\Psi_b(x) \\ & \qquad - j\lambda\alpha^*\beta^*\Omega\cdot\cos(\omega_m t)B(t)\Psi_a(x) \\ & \qquad + \Big[(j\omega_b - \Gamma_b) - j\lambda(\alpha^*\alpha - \beta^*\beta)\Omega \\ & \qquad\quad \cdot\cos(\omega_m t)/2\Big]B(t)\Psi_b(x)\Bigg\} \\ & \qquad \times \exp(j\omega_P t - \Gamma_P t). \end{aligned}$$

Collecting together the terms in Ψ_a and Ψ_b gives

$$\begin{aligned}&\partial A(t)/\partial t + (j\omega_P t - \Gamma_P)A(t)\\&\quad = \Big[j\omega_a - \Gamma_a + j\lambda(\alpha^*\alpha - \beta^*\beta)\Omega\cos(\omega_m t)/2\Big]A(t)\\&\qquad - j\lambda\alpha^*\beta^*\Omega\cos(\omega_m t)B(t)\\&\partial B(t)/\partial t + (j\omega_P t - \Gamma_P)B(t)\\&\quad = -j\lambda\alpha\beta\Omega\cos(\omega_m t)A(t)\\&\qquad + \Big[j\omega_b - \Gamma_b - j\lambda(\alpha^*\alpha - \beta^*\beta)\Omega\cos(\omega_m t)/2\Big]B(t).\end{aligned}$$

The second of these equations shows that $B(t)$ is smaller than $A(t)$ by the parameter λ and, hence, the term involving $B(t)$ in the first equation can be ignored to first order in λ. The reduced first equation can now be separated in two parts to give

$$(j\omega_P - \Gamma_P) = (j\omega_a - \Gamma_a)$$

and

$$\partial A(t)/\partial t = \Big[j\lambda(\alpha^*\alpha - \beta^*\beta)\Omega\cos(\omega_m t)/2\Big]A(t)$$

hence,

$$\begin{aligned}&A(t)\\&\quad = 1 + j\lambda(\alpha^*\alpha - \beta^*\beta)\Omega\sin(\omega_m t)/2\omega_m\\&\quad = 1 + \lambda(\alpha^*\alpha - \beta^*\beta)\Omega\Big[\exp(j\omega_m t) - \exp(-j\omega_m t)\Big]\Big/4\omega_m\end{aligned}$$

which describes a phase modulation of the part of Ψ_P that is associated with $\Psi_a(x)$. The second equation may be reorganized to give

$$\begin{aligned}&\partial B(t)/\partial t + \Big[j\omega_a - \Gamma_a - j\omega_b + \Gamma_b\Big]B(t)\\&\qquad = -j\lambda\alpha\beta\Omega\Big[\exp(j\omega_m t) + \exp(-j\omega_m t)\Big]\Big/2\end{aligned}$$

where the term $j\lambda(\alpha^*\alpha - \beta^*\beta)\Omega\cdot\cos(\omega_m t)B(t)/2$ has been dropped as second order in λ, $j\omega_P - \Gamma_P$ has been replaced by $j\omega_a - \Gamma_a$ and $A(t)$ by one. This equation shows that $B(t)$ has two parts $B_+(t)$ and $B_-(t)$ associated with the two terms $+j\omega_m$ and $-j\omega_m$, which are solutions to the equations

$$\begin{aligned}&\partial B_\pm(t)/\partial t + \Big[j\omega_a - \Gamma_a - j\omega_b + \Gamma_b\Big]B_\pm(t)\\&\qquad = -j\lambda\alpha\beta\Omega\exp(\pm j\omega_m t)\Big/2\end{aligned}$$

hence,

$$\begin{aligned}B_\pm(t) = -\frac{1}{2}\lambda\alpha\beta\Omega\exp(\pm j\omega_m t)\Big/\\\Big[\omega_a - \omega_b \pm \omega_m + j\Gamma_a - j\Gamma_b\Big].\end{aligned}$$

The amplitude of the wave in the second resonator $A_2(t)$, which determines the outgoing flux, is given by $\beta A(t) + \alpha^* B(t)$. Substituting for $A(t)$ and $B(t)$ gives

$$\begin{aligned}A_2(t) = \beta\Bigg[1 + \frac{1}{4}j\lambda(\alpha^*\alpha - \beta^*\beta)\Omega\sin(j\omega_m t)/\omega_m\\ - \frac{1}{2}\lambda\alpha^*\alpha\Omega\exp(+j\omega_m t)\Big/\\(\omega_a - \omega_b + \omega_m + j\Gamma_a - j\Gamma_b)\\ - \frac{1}{2}\lambda\alpha^*\alpha\Omega\exp(-j\omega_m t)\Big/\\(\omega_a - \omega_b - \omega_m + j\Gamma_a - j\Gamma_b)\Bigg].\end{aligned}$$

In this equation, the second term describes a phase modulation that decreases as ω_m is increased, this phase modulation is that which is given by the change in the frequencies ω_a and ω_b of the two modes as a result of the perturbation. The last two terms describe a modulation that is resonantly peaked when $\omega_m = |\omega_a - \omega_b|$. As ω_m is swept through this resonance, the phase of this modulation will change, and the modulation will vary from being chiefly amplitude modulation far from resonance to phase modulation exactly on resonance. The maximum degree of amplitude modulation is given when $|\omega_a - \omega_b \pm \omega_m| = |\Gamma_a - \Gamma_b|$. If the system is such that $|\beta| \ll |\alpha| \sim 1$, then the maximum degree of amplitude modulation is given by $1/4\lambda\Omega/|\Gamma_a - \Gamma_b|$. This can be compared with the change in A_2 that would be produced by the static perturbation $\lambda\Omega$, which is equal to $\lambda\Omega/(\omega_1 - \omega_2 + j\Gamma_1 - j\Gamma_2)$. This comparison shows that a perturbation four times as large is required to produce a given degree of modulation in the amplitude A_2 under conditions of maximum resonant modulation compared with that required when $\omega_1 = \omega_2$; this result will be used in the analysis of the experimental data presented later in this paper.

This analysis shows that a wave emerging from a filter structure can be modulated at a higher frequency than the intrinsic bandwidth of one of the filter modes by resonant coupling to a second mode of the filter. Modulation is achieved by changing the resonant frequency of the second mode at the required modulation frequency. In any such system, there is a resonant enhancement of the degree of modulation when the modulation frequency is equal to the difference in the resonant frequencies of the two modes. The mathematics of this result is quite general and can be applied to any system in which a pair of resonators are weakly coupled to an input and output and to each other. Numerical modeling of systems with three quantum wells, which correspond to a six-pole filter show that, with the right arrangement of poles, the phase part of the modulation may be cancelled and the amplitude modulation enhanced to give an even higher modulation gain.

The analysis presented above considered the two natural modes of the filter. If the system is used to modulate a continuous wave, then the unperturbed function will have a fixed frequency ω_0, which will replace, in the analysis, the term $\omega_a + j\Gamma_a$. The continuous wave will excite to some degree both the modes Ψ_a and Ψ_b, to extents which depend on the difference between its frequency ω_0 and those of the two modes ω_a and ω_b. Resonant amplification of the degree of modulation may be observed when $\omega_m = |\omega_a - \omega_0|$ and also when $\omega_m = |\omega_b - \omega_0|$. Since the unmodulated continuous wave state has no damping, the degree of modulation is proportional to $\lambda\Omega/(\omega_a - \omega_o \pm \omega_m + j\Gamma_a)$ or $\lambda\Omega/(\omega_b - \omega_o \pm \omega_m + j\Gamma_b)$; this implies that the damping of the each of the separate modes determines the degree of resonant enhancement.

In the triple-barrier device, the incoming electrons have a broad spectrum of energies. The overall effect of the modulator on the electron current is found be calculating the modulation characteristics for each possible incident electron energy and then integrating the overall modulation assuming random phases for the different electron waves. Since the outgoing electron flux is dominated by the energies of the two passbands of the triple-barrier structure, the modulation characteristics also

reflect these passbands. In the particular triple-barrier structures described in this paper, the passband associated with the first well is dominant and the modulation properties obtained by integrating the modulation equations over the width of the passband. To a good approximation, this gives a degree of modulation proportional to $\lambda\Omega/(\omega_a - \omega_b + \omega_m - j\Gamma_a - j\Gamma_b)$; implying that the damping of both modes determines the resonant enhancement in the modulation.

The significance of this calculation for terahertz devices can now be presented. Due to the mass of the electron, there is a limit, both empirical and theoretical, to the energy width and, hence, bandwidth, of an electron state in the quantum well of a DBRTS device. In order to achieve oscillation or amplification at frequencies over 1 THz, it is necessary to use the extension of the bandwidth of tunneling devices provided by the QMIST effect. If an ac electric field is applied, whose frequency is near to that which corresponds to the difference between the energies of the quasi-confined states of the two wells, then the effect of the electric field will be to drive charge in an oscillatory fashion between the emitter and collector wells. Since the device is designed so that the amplitude of the wave in the first emitter well A_1 and, hence, the electron density, is significantly higher than in the second collector well, a relatively small fractional change in this electron density will produce a much larger fractional change in the collector well electron density and, hence, a significant change in the collector current. The analysis shows that the maximum in the amplitude of $B(t)$ occurs when $|\omega_a - \omega_b| = \omega_m$, and that the phase of $B(t)$ lags the perturbation by 90°, a situation which corresponds to maximum power absorption by the oscillating electron density at resonance. The external device current is determined by $B(t)$, and a phase shift greater than 90° is required for there to be a component in this external current that is out of phase with the perturbation and, hence, feeds power into the source of the perturbation. The maximum in the negative conductance of a triple-barrier QMIST device will occur at the frequency that exceeds that corresponding to the difference in the two state energies by about half the bandwidth of the interstate resonance, a condition giving a 135° phase shift between the collector current and the ac bias.

III. Structures and Devices

Wafers were grown in the GaAs/AlGaAs system on semi-insulating GaAs substrates using molecular beam epitaxy in a VG Semicon V90H system. This system gives better than 1% thickness and doping uniformity across 50-mm wafers and a background doping density around 10^{14} cm^{-3}. The growth was conducted with a near stochiometric flux ratio, which allowed low growth temperatures (580–540 C) and high densities of active silicon n-type dopant. A typical structure included the following layers: n^{++} bottom contact layer (1-μm thick, Si 3×10^{18} cm^{-3}), a spacer layer (10 nm, Si 1×10^{17} cm^{-3} and 10 nm, undoped), first barrier (4.5 nm, undoped $Ga_{0.67}Al_{0.33}As$), first well (6.5 nm, undoped), second barrier (5.4 nm, undoped $Ga_{0.67}Al_{0.33}As$), second well (5.4 nm, undoped), third barrier (4.5 nm, undoped $Ga_{0.67}Al_{0.33}As$), spacer layer (20 nm, undoped), n delta doped layer (Si 1×10^{12} cm^{-2}), n^{++} upper contact (0.5 μm, Si 7×10^{18} cm^{-3}). A number of parameters were varied, including the aluminum mole fraction in the barriers, but the variable whose effect was most closely studied was the width of the second well, which ranged from 6.8 to 4.2 nm over a series of ten wafers. Fig. 1 shows energies of the quasi-confined levels and the band edge of one of the structures under bias.

Isolated devices were made from all of these structures: the devices were in the form of a double mesa with an active area approximately 80-μm square. AuGe/Ni/Au ohmic contacts were made to both the top and bottom contact layers, which were exposed on the two mesa steps. The upper contact had an optical window so that optical studies could be conducted in the presence of current flow.

IV. Structure Characterization

The objective in designing triple-barrier structures for terahertz applications is to ensure that, with a bias which lowers the energy of the emitter-well quasi-confined state to equal that of the emitter conduction band edge, the energy separation between the two quasi-confined states has the appropriate value for the desired operating frequency. The former condition corresponds to the highest dc current density and the latter to the maximum resonant enhancement of the power gain of the device. It follows that the absolute and relative electron confinement energies of the two wells need to be measured if the suitability of any triple-barrier structure for a particular terahertz application is to be assessed. In simple quantum-well structures, photoluminescence spectroscopy is used to measure the confined electron–hole transition energies, allowing the electron confinement energies to be deduced. An intrinsic property of high-speed tunneling structures is that the electron and hole escape times from the quantum wells are very short; these will, therefore, be a very small fraction of the time taken for radiative electron–hole recombination. It follows that little if any intensity can be expected at wavelengths corresponding to the well transitions, and none has been observed in our samples. A novel method of photoluminescence excitation spectroscopy, which we have developed, has been used to measure the well transition energies. This technique has been applied to as-grown wafers and yielded good results for all our structures. In it, any optical radiation from the structure at the wavelength for emission from the heavily doped contact region of the structure is monitored: this region is where holes, optically generated in the wells, will recombine after tunneling through the barriers. The output of a tunable laser is directed on to the sample (usually cooled to 6 K in most of our experiments) and the wavelength of this light is scanned over the range of the well transitions. Clear signals of an excitonic character have been observed when the incident light has an energy corresponding to any of the lowest electron-heavy hole or electron-light hole transitions in the wells of the sample. We have used the electron confinement energies deduced from these to characterize the samples and to provide rapid feedback to the grower. Fig. 2 shows examples of such spectra for a number of our structures. This figure shows two very significant characteristics: first, it is possible to assess the confinement energies and well widths from these spectra and, second, that the spectra

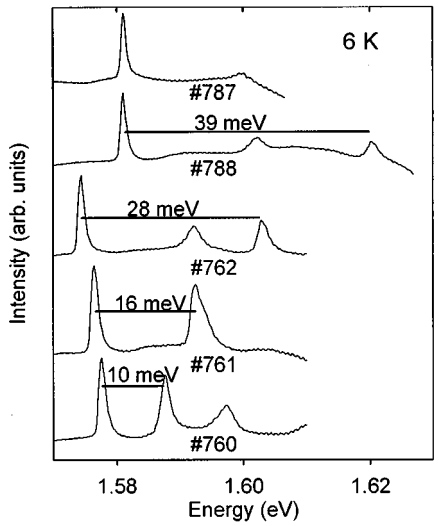

Fig. 2. Optical spectra from zero-bias characterization (photoluminescence excitation at 6 K) from a series of triple-barrier structures in which only one well width was deliberately varied. The resonant electron state in each well gives rise to two spectral transitions separated by about 20 meV. The data show the degree of control that can be achieved in crystal growth by molecular beam epitaxy over the electronically important parameters of the energy and half-width of the electron states in the quantum wells.

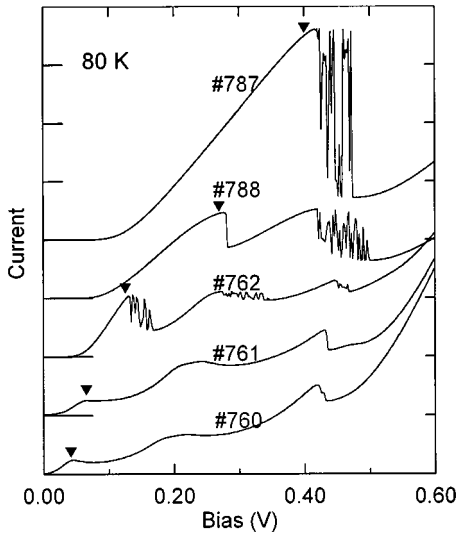

Fig. 3. Forward-bias current–voltage curves measured at 80 K for a number of 80-μm square triple-barrier devices. The solid inverted triangles indicate the bias at which the two resonant electron states are aligned. Operation as a terahertz device occurs at biases a few hundredths of a volt below this. The zero current ordinate is shifted up by one division for each data set, corresponding to 10 mA for the lower three curves and 30 mA for the upper two curves.

provide a direct confirmation that the energies of the quasi-confined states are well defined in our structures with linewidths from 1.0 to 2.0 meV. (corresponding to 250–500 GHz)

V. Level Crossing Effects

A separation in energy of a few millielectronvolts between the two quasi-confined states is required for the resonant enhancement of the negative conductance of the devices to occur at terahertz frequencies. It is clearly useful to be able to identify the features that are characteristic of the alignment of these two energies so that the bias can then be adjusted by the appropriate amount to achieve this spacing. Our experimental studies of a series of triple-barrier tunneling structures over the wide range of temperatures 13–300 K, supplemented by numerical calculations based on a physical device model, have established that the current reaches a peak at the bias at which the energies of the states are aligned [3]. This is a direct consequence of the integrated transparency of a triple-barrier structure having its maximum value when the energies of the quantum states are aligned. Fig. 3 shows the current–voltage characteristics measured on three different structures at a temperature of 80 K. The currents at the biases indicated have the temperature dependence that is predicted for the current at the alignment of the two energies and occurs at a bias that corresponds to the calculated bias for this alignment. It follows that the bias required for the alignment of the energy levels in any structure can be determined if such a feature can be identified. The figure also shows that a structure with a greater difference in the confinement energies of the two wells requires a greater bias to produce the alignment and gives, for similar emitter-well confinement energies, a higher device current at alignment since the energies of the two well states under these conditions are closer to the Fermi level in the emitter. The terahertz negative conductance is a resonant enhancement of the dc conductance; it follows that an optimized device will have as large a current density as possible and will, therefore, operate with a bias as close as possible to that which aligns the emitter-well energy with the peak electron density in the emitter. This is the origin of the first structural requirement stated in Section IV.

Once sufficient bias is applied to a device, an electron current will flow from the emitter to the collector, and any holes generated in the collector, for example by an external light source as in a conventional photoluminescence experiment, would be transported toward the emitter. Under these conditions, the quantum wells would have a steady-state population of both electrons and holes, and optical radiation with wavelengths characteristic of the quantum wells should be observable. Such radiation has been studied for our devices for which the upper collector contact was illuminated by a laser. The variation with bias of the wavelengths and line shapes give important information about the internal behavior of the devices [4]. The data shown in Fig. 4 is the most significant for assessing the terahertz behavior of these devices. The two curves in the upper part of the figure show the integrated light output characteristic of the emitter and collector wells as a function of bias, while the curve in the lower part shows the current–voltage characteristic. The intensity of the output from either well is a function of a number of parameters including the product of the electron and hole densities. The significant feature in this diagram is the abrupt dip at a bias of 0.12 V in the intensity of the light arising from the emitter well. This bias also corresponds to that at which the energies of the two quasi-confined states are aligned. The theoretical model predicts that the electron density in the emitter well falls when the energies of these two electron states are aligned; we interpret this fall in the intensity of the light as a decrease in the electron density in the emitter well caused by the alignment of the two

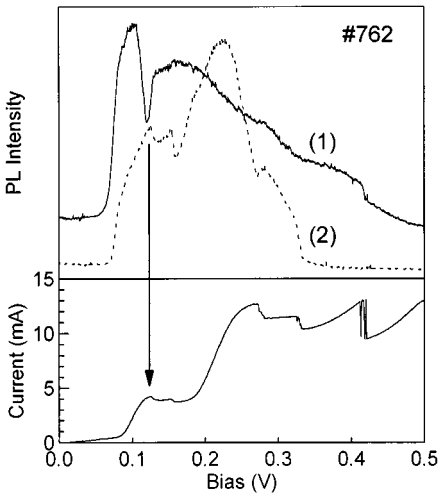

Fig. 4. Upper part shows the variation with bias of the integrated optical output characteristic of the product of the electron and hole densities in the emitter well (continuous line) and the collector well (dotted line) in a photoluminescence experiment on a single device of structure #762 at 6 K. The lower part shows the current–voltage characteristic of the device measured at the same time.

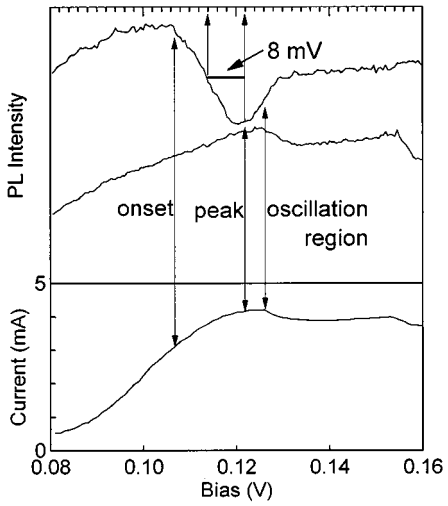

Fig. 5. Portion of the data from Fig. 4 showing in detail the dip in the optical output from the emitter well around a bias of 0.12 V.

energies. The significant feature for the prediction of the terahertz behavior of these devices is the bias range over which the charge decreases: this is shown in detail in Fig. 5. The half-width in bias of the charge decrease is 16 mV. This is consistent with the observed energy half-widths measured for the two electron states in this sample, namely, 1.3 and 2.0 meV, and the measured ratio of 6.0:1 between a change in the applied bias and the relative energies of the two well states.

One of the difficulties in theoretically modeling the response of the device at high frequencies is the need to make self-consistent calculations of the field and resultant charge distribution that feed back on each other. The experimentally observed drop in electron density on level crossing is subject to the same degree of feedback. An experimental measurement of the range of bias over which this drop is observed, therefore, includes directly any extra effects associated with electrostatic feedback on the field distribution produced from the applied bias caused by changes in the electron distribution.

VI. Terahertz Behavior

In addition to finding the condition for maximum negative conductance, it is necessary to determine the expected magnitude of this conductance, which can be found from the ac bias that would give 100% modulation of the collector current in a linear model. The data of Fig. 5 is most significant in making this estimate. The fall in charge in the emitter well is equivalent to the ac resonance for zero frequency and theoretical models show that the conductances for these two cases are comparable, but with the ac resonant effect smaller by a factor of four, as has been demonstrated in the theoretical section. We, therefore, estimate that, for our structures, an rms bias of 50 mV should modulate the collector current between 200% and 0% of its dc value giving an rms ac current of 70% of the static value. The device structure with the highest current density, i.e., #787, has a peak current density of over 1.5×10^3 A/cm^2; for this structure, the calculated maximum negative conductance is 2×10^4 S/cm^2. A negative conductance of -0.02 S required to drive a 50-Ω system would require a device area of 100 μm^2. The typical depletion length in our structures is 66 nm as determined from the ratio of the change between different structures in the bias required to align the two energy levels to the change in the zero-bias splitting of these levels. The capacitance for a 100 μm^2 device with this depletion distance would be 170 fF; such a device would have an impedance at 1 THz of 0.8 Ω. The matching circuit for this device would, therefore, need a Q of 60 in a 50-Ω environment. The bias at which this resonance would be seen would be about 20 mV below the current peak.

The construction of a matching circuit with a Q of 60 at 1 THz is probably beyond current technologies; however, the specific negative conductance is controlled by the current density, which is, in turn, determined by the tunneling rate through the barriers. The structures for which data have been presented in this paper were designed to meet the requirements for optical measurements. These need reasonable ($<$0.5 A) bias currents for devices with an area comparable to the 75-μm diameter of the image of the illuminating laser. Much greater current densities have been reported for double-barrier tunneling devices fabricated from GaAs with AlAs barriers [5]; it is reasonable to expect that ratios of conductance to capacitance could be achieved which are at least ten times those reported here. It should be easy to match such devices to a 50-Ω environment; they, therefore, have considerable potential as the basis for practical sources of power in the 1–3-THz range.

VII. Conclusion

A theoretical description of a resonantly enhanced modulator has been presented in this paper. This modulator is the basis for a series of triple-barrier devices that are intended to act as oscillators and amplifiers at terahertz frequencies. Results of measurements on the devices have been analyzed to assess their probable performance at frequencies around 1 THz. There is good experimental evidence that the structures would exhibit a resonantly enhanced negative conductance in this frequency range. It is apparent that one existing structure could be used as a power

source if good matching of the structural capacitance could be achieved. Future developments of these devices are likely to improve the ratio of the negative conductance to capacitance; this would allow matching over a broader range of frequencies.

REFERENCES

[1] W. S. Truscott, "Negative conductance at THz frequencies in multi-well structures," *Solid State Electron.*, vol. 37, pp. 1235–1238, 1994.
[2] E. R. Brown, J. R. Soderstrom, C. D. Parker, J. L. Mahoney, K. M. Molvar, and T. C. McGill, "Oscillations up to 712 GHz in InAs/A1Sb resonant-tunneling diodes," *Appl. Phys. Lett.*, vol. 58, pp. 2291–2293, 1991.
[3] C.-Y. Kuo, M. A. Lynch, A. H. Roberts, P. D. Buckle, P. Dawson, M. Missous, and W. S. Truscott, "An electrical and optical study of electrons in triple barrier structures," *Physica E*, vol. 2, pp. 815–819, 1998.
[4] P. D. Buckle, P. Dawson, C.-Y. Kuo, A. H. Roberts, W. S. Truscott, M. Lynch, and M. Missous, "Charge accumulation in GaAs/A1GaAs triple barrier resonant tunneling structures," *J. Appl. Phys.*, vol. 83, pp. 882–887, 1998.
[5] L. Yang, D. E. Mars, and M. R. T. Tan, "Effect of electron launcher structures on A1As/GaAs double barrier resonant tunneling diodes," *J. Appl. Phys.*, vol. 73, pp. 2540–2542, 1993.

Philip D. Buckle, photograph and biography not available at time of publication.

Philip Dawson, photograph and biography not available at time of publication.

Mark A. Lynch, photograph and biography not available at time of publication.

Chun-Yi Kuo, photograph and biography not available at time of publication.

Mohammed Missous, photograph and biography not available at time of publication.

William S. Truscott, photograph and biography not available at time of publication.